# Milankovitch Forcing and Meridional Moisture Flux in the Atmosphere: Insight from a Zonally Averaged Ocean–Atmosphere Model

ANDRÉS ANTICO

*Department of Atmospheric and Oceanic Sciences, McGill University, Montreal, Quebec, Canada*

OLIVIER MARCHAL

*Department of Geology and Geophysics, Woods Hole Oceanographic Institution, Woods Hole, Massachusetts*

LAWRENCE A. MYSAK

*Department of Atmospheric and Oceanic Sciences, McGill University, Montreal, Quebec, Canada*

FRANÇOISE VIMEUX

*Institut de Recherche pour le Développement (IRD), Laboratoire HydroSciences Montpellier, UMR 5569, and Laboratoire des Sciences du Climat et de l'Environnement, UMR 8212, Gif-sur-Yvette, France*

(Manuscript received 2 June 2009, in final form 11 April 2010)

ABSTRACT

A 1-Myr-long time-dependent solution of a zonally averaged ocean–atmosphere model subject to Milankovitch forcing is examined to gain insight into long-term changes in the planetary-scale meridional moisture flux in the atmosphere. The model components are a one-dimensional (latitudinal) atmospheric energy balance model with an active hydrological cycle and an ocean circulation model representing four basins (Atlantic, Indian, Pacific, and Southern Oceans). This study finds that the inclusion of an active hydrological cycle does not significantly modify the responses of annual-mean air and ocean temperatures to Milankovitch forcing found in previous integrations with a fixed hydrological cycle. Likewise, the meridional overturning circulation of the North Atlantic Ocean is not significantly affected by hydrological changes. Rather, it mainly responds to precessionally driven variations of ocean temperature in subsurface layers (between 70- and 500-m depth) of this basin. On the other hand, annual and zonal means of evaporation rate and meridional flux of moisture in the atmosphere respond notably to obliquity-driven changes in the meridional gradient of annual-mean insolation. Thus, when obliquity is decreased (increased), the meridional moisture flux in the atmosphere is intensified (weakened). This hydrological response is consistent with deuterium excess records from polar ice cores, which are characterized by dominant obliquity cycles.

## 1. Introduction

Long-term variations in the geometry of Earth's orbit around the Sun produce changes in the incoming solar radiation (i.e., insolation), which is the main external forcing of the climate system. These variations consist of the precession of the equinoxes (dominant periods of 19 and 23 kyr), obliquity cycles (41 kyr), and eccentricity cycles (100 and 400 kyr). The resulting insolation cycles are known as Milankovitch forcing (see Loutre et al. 2004 and Crucifix et al. 2006 for a detailed description). Precession modifies the amplitude of the seasonal cycle of insolation without changing the annual-mean insolation. Obliquity changes the meridional gradient of annual-mean insolation without modifying the global-mean insolation. Eccentricity modulates the precessionally driven insolation changes and produces small variations of the global- and annual-mean insolation. Whereas the Milankovitch forcing can be accurately computed through astronomical calculations (e.g., Berger 1978; Berger and Loutre 1991), the climatic response to it is not completely understood (for a review see Paillard 2001). A better understanding of this response, however, is necessary to

*Corresponding author address:* Andrés Antico, Dept. of Atmospheric and Oceanic Sciences, McGill University, 805 Sherbrooke St. West, Montreal QC H3A 2K6, Canada.
E-mail: andres.antico@mail.mcgill.ca

DOI: 10.1175/2010JCLI3273.1

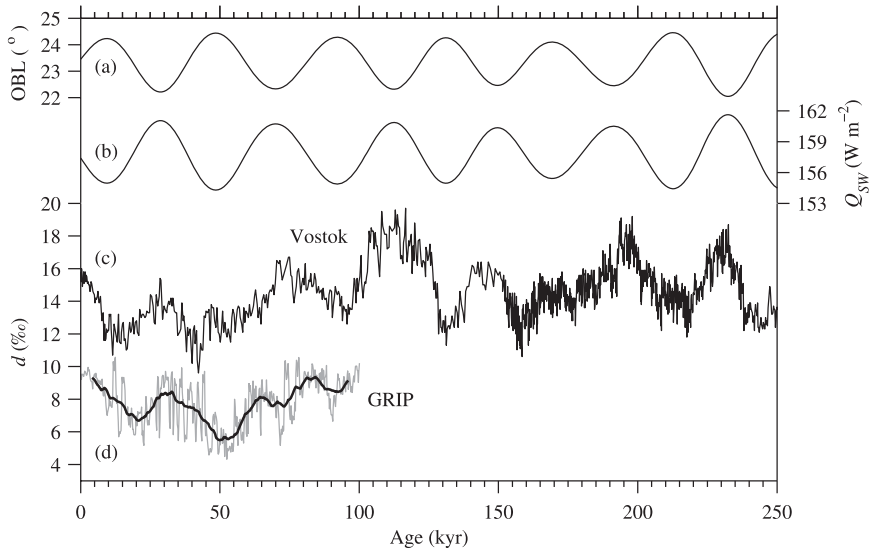


FIG. 1. Time series of (a) obliquity, (b) difference in annual-mean insolation between 20° and 60°S, (c) deuterium excess from Vostok ice core (Vimeux et al. 2001a), and (d) deuterium excess from Greenland Ice Core Project (GRIP; Masson-Delmotte et al. 2005). In plot (d), raw data are shown by the gray line and an 8-kyr moving average is shown by the black line.

properly interpret paleoclimate records that contain variability near Milankovitch frequencies (e.g., Tiedemann et al. 1994; Petit et al. 1999; Vimeux et al. 1999, 2001a; Masson-Delmotte et al. 2005; Lisiecki and Raymo 2005, 2007; Jouzel et al. 2007).

Numerical models have been used to gain insight into the response of the earth's climate to Milankovitch forcing. However, this still is a challenging exercise because of computing limitations and our incomplete understanding of several climatic processes (Valdes and Glover 1999). Equilibrium or quasi-equilibrium solutions for a fixed Milankovitch forcing have been obtained with general circulation models (GCMs; e.g., Braconnot et al. 2000; Khodri et al. 2001). In this manner, it is possible to obtain detailed simulations of a climate system that is in near equilibrium with a seasonal cycle of insolation for a particular year. Ideally, GCMs should also be used for obtaining long (e.g., 1 Myr) time-dependent solutions. However, these models are too computationally expensive for such numerical experiments and, therefore, are not suitable for studying the time-dependent response of climate to Milankovitch forcing. Hence, simplified and computationally efficient climate models are used to simulate this climatic response. For instance, Brickman et al. (1999) were the first to perform a 3.2-Myr-long integration with a modified version of the zonally averaged ocean–atmosphere model of Stocker et al. (1992b) under the influence of Milankovitch forcing. They analyzed global and annual averages of climatic variables (e.g., air and ocean temperatures). Recently, this pioneering work was extended by Antico et al. (2010, hereafter referred to as AMM10), who generated 2-Myr-long time-dependent solutions of a zonally averaged ocean–atmosphere–sea ice model. AMM10 investigated the responses to Milankovitch forcing of (i) air and ocean temperatures at different locations and (ii) sea ice. Interestingly, the results of AMM10, which are in agreement with those of Brickman et al. (1999), show different responses in the ocean and the atmosphere. For example, while surface air temperature mainly responds to obliquity, deep ocean temperature notably responds to precession.

It is important to note that the climate models of Brickman et al. (1999) and AMM10 neglect several climatic components. In particular, a time-varying meridional moisture flux in the atmosphere was not considered in both studies (i.e., an active hydrological cycle was not included). Several studies have proposed that this flux mainly responds to obliquity (e.g., Young and Bradley 1984) or to the meridional gradient of air temperature (e.g., Stone and Miller 1980; Rind 1998). (This gradient can also be controlled by obliquity, e.g., AMM10.) In fact, some paleoclimate records suggest the existence of such a hydrological response to obliquity. For example, deuterium excess from polar ice cores, which is believed to reflect changes in the atmospheric poleward moisture flux (Vimeux et al. 1999, 2001a), tends to follow obliquity-driven changes in the meridional gradient of annual-mean insolation (Fig. 1). In view of these proposed and recorded hydrological changes on Milankovitch

time scales, it is of interest to repeat the numerical experiment of AMM10 but with an active hydrological cycle. The question of whether this inclusion would fundamentally modify the results of AMM10 cannot be answered by intuition because of the complex interactions between the hydrological cycle and other climatic elements. For instance, the equilibrium states of a zonally averaged ocean–atmosphere model and the transition between them significantly change when an active hydrological is incorporated in the model (Bjornsson et al. 1997).

In this paper, we extend the model of AMM10 to include an active hydrological cycle. The new model is then integrated under the influence of Milankovitch forcing over the last 1 Myr (i.e., late Pleistocene). In this manner, we gain insight into long-term hydrological changes and their role in the response of the ocean–atmosphere system to Milankovitch forcing.

Several simplifications are introduced into our model to increase the computational efficiency and facilitate the identification of fundamental aspects of the climatic response to Milankovitch forcing. One obvious limitation is the zonal averaging of the governing equations. Furthermore, climate components such as sea ice, the biosphere (e.g., carbon cycle), and continental ice sheets are not represented. Thus, our model best represents warm climates (i.e., with negligible ice volume on land). Nevertheless, numerical experiments bearing on warm climates already prove to be useful for improving our understanding of the response of climate to Milankovitch forcing (e.g., Park and Oglesby 1990; Short et al. 1991; Valdes et al. 1995; Brickman et al. 1999; Khodri et al. 2001; Crucifix and Loutre 2002; AMM10).

The rest of the paper is organized as follows. The climate model and experimental design are described in sections 2 and 3, respectively. Results from the time-dependent solution are reported in section 4 and discussed in section 5. Finally, conclusions are provided in section 6.

## 2. Model description

A detailed description of the model is given in AMM10. Only a brief overview of the model components is provided here, except for the hydrological cycle. The zonally averaged ocean circulation model of Wright and Stocker (1992) is implemented in four basins (Atlantic, Indian, Pacific, and Southern Oceans) and coupled to a zonally averaged one-dimensional (latitudinal) energy balance model of the atmosphere. This atmospheric component is extended here to include a simple representation of an active hydrological cycle as described later in this section. Note that our hydrological component does not include (i) important hydrological processes in the Arctic Basin (e.g., river runoff), where most of the Northern Hemisphere sea ice exists, and (ii) a representation of snowfall. Thus, we use a model version without sea ice and the Arctic Ocean [the model domain is as in the NOICE experiment (i.e., the model run with no sea-ice component) of AMM10].

The hydrological cycle model is similar to that of Schmittner and Stocker (1999). Assuming steady state, the divergence of the meridional flux of water vapor is balanced by the sources and sinks of moisture:

$$\frac{1}{R^2}\frac{\partial L_i}{\partial s} - \rho_0 \sum_{j=1}^{n} (E_{ij} - P_{ij}) \frac{\Delta\Lambda_{ij}}{2\pi} = 0. \tag{1}$$

Here, the index $i$ ($j$) denotes the dependency on latitude (ocean basin), $n$ is the total number of ocean basins at a given latitude, $R$ is the earth's radius, $L$ is the meridional flux of water vapor, $s$ is the sine of latitude, $\rho_0$ is a reference density of seawater, $E$ ($P$) is the evaporation (precipitation) rate, and $\Delta\Lambda$ is the ocean basin angular width.

The hydrological variables in Eq. (1) are estimated as follows. The meridional transport of water vapor is parameterized as (e.g., Schmittner et al. 2000)

$$L_i = -\rho_a H_q c^2 K_i \left|\frac{\partial T_a^i}{\partial s}\right| \frac{\partial q_i}{\partial s}, \tag{2}$$

where $\rho_a$ is a reference density of air, $H_q$ is a scale height for humidity, $c$ is the cosine of latitude, $K$ is a time-invariant mixing coefficient (described below), $T_a$ is the zonal-mean (over entire latitudinal circles) surface air temperature, and $q$ is the specific humidity. The latter is calculated as $q = rq_s(T_a)$, where $r$ is the relative humidity (considered constant) and $q_s$ is the saturation specific humidity (a function of temperature as in AMM10). In Eq. (2), $L$ is given in kg s$^{-1}$ and can be converted to meridional flux of latent heat by multiplying it by the latent heat of evaporation ($L_0$).

The local evaporation rate $E_{ij}$ is computed from a bulk formula, namely,

$$E_{ij} = \frac{\rho_a}{\rho_o} C_E^{ij} W^{ij} [q_s(T_m^{ij}) - q_i], \tag{3}$$

where $C_E$ is a transfer coefficient for moisture (described in appendix C of AMM10), $W$ is the monthly climatological mean of wind speed at an elevation of 10 m (Kalnay et al. 1996), and $T_m$ is the ocean mixed layer temperature.

The local precipitation rate $P_{ij}$ during a coupled run is calculated as follows. Given $K_i$ and the modeled temperatures $T_a^i$ and $T_m^{ij}$, Eq. (1) can be solved for the zonal average of $P_{ij}$ ($=\overline{P}_i$; henceforth, the overbar denotes a zonal average). An assumption needs to be made to

partition the precipitation rate $\overline{P}_i$ among different ocean basins. According to the scheme P1 of Schmittner and Stocker (1999), the distribution of $\overline{P}_i$ into different basins is assumed to be equal to the zonal distribution of annual-mean precipitation diagnosed at the end of the ocean model spinup under restoring boundary conditions for surface temperature and salinity (the ocean model spinup is described in the appendix). This diagnosed precipitation ($P^*_{ij}$) is obtained from the annual-mean sea surface freshwater flux at the end of the ocean model spinup and from the annual climatological mean of evaporation (Kalnay et al. 1996). Alternatively, one could use the closure P2 of Schmittner and Stocker (1999), in which $\overline{P}_i(t) = \overline{P}^*_i + \overline{P}'_i(t)$, where $\overline{P}^*_i$ is the zonal average of $P^*_{ij}$; and $\overline{P}'_i(t)$ a time-dependent anomaly. This equation is solved for $\overline{P}'_i(t)$, and a local precipitation anomaly $P'_{ij}(t)$ is obtained by assuming that $\overline{P}'_i(t)$ is uniformly distributed among the different ocean basins. Then, the local precipitation is estimated as $P_{ij} = P^*_{ij} + P'_{ij}(t)$. In this work, similar results were obtained with P1 and P2. Only results obtained with P1 are shown and discussed below.

In a coupled run, the modeled $E_{ij}$ and $P_{ij}$ are used to calculate the sea surface salt flux $F_S$ as $F_S = S_0(P - E)_{ij}$, where $S_0$ is a reference salinity.

Consider now the mixing coefficient $K_i$, which is determined at the end of the ocean model spinup under restoring boundary conditions for surface temperature and salinity. Given the annual mean $(P - E)_{ij}$ diagnosed at the end of the ocean model spinup and the annual climatological mean of $T^i_a$ (Kalnay et al. 1996), Eq. (1) can be solved for $K_i$:

$$K_i = \frac{\rho_0 R^2}{\rho_a H_q c^2 \left|\frac{\partial T^i_a}{\partial s}\right| \frac{\partial q_i}{\partial s}} \int_{-1}^{s} \left[\sum_{j=1}^{n} (P - E)_{ij} \frac{\Delta\Lambda_{ij}}{2\pi}\right] ds. \quad (4)$$

In this manner, negative $K_i$ values are only obtained at 7.5°S and 7.5°N. These negative $K_i$ are replaced by $K_i = 100\ \mathrm{m^2\ (s\ K)^{-1}}$. As noted by Schmittner et al. (2000), the occurrence of negative $K_i$ values near the equator shows that representing the meridional humidity transport as a purely diffusive process is not appropriate at low latitudes.

The spinup procedure and an equilibrium solution for present-day climate are described in the appendix. All the model parameters are as in AMM10, except those of the hydrological cycle component, which are given in Table 1.

TABLE 1. Parameters in the hydrological cycle component.

| | | |
|---|---|---|
| $R$ | Earth's radius | 6371 km |
| $H_q$ | Atmospheric scale height for humidity | 1800 m |
| $r$ | Relative humidity | 0.85 |
| $\rho_a$ | Reference density of air | 1.225 kg m$^{-3}$ |
| $\rho_o$ | Reference seawater density | 1028 kg m$^{-3}$ |
| $L_0$ | Latent heat of evaporation | $2.5 \times 10^6$ J kg$^{-1}$ |
| $S_0$ | Reference salinity | 34.7 PSU |
| $C_E$ | Air–sea transfer coefficient for moisture* | $(1.6 - 9.2) \times 10^{-3}$ |
| $K$ | Mixing coefficient for humidity** | $(10^{-3} - 1.1) \times 10^5$ m$^2$ (s K)$^{-1}$ |

* Determined as described in appendix C of AMM10.
** See section 2 of this paper for details.

## 3. Experimental design

The model is integrated to produce a time-dependent solution for the last 1 Myr. The initial conditions consist of an equilibrium solution for modern climate (appendix), and the model is forced with a time-varying latitudinal distribution of insolation (Berger 1978).

Several model outputs are saved every 2 kyr (e.g., spatial distributions of annual and zonal means of air and ocean temperatures and evaporation rate) or every 200 yr (e.g., annual-mean streamfunction in the Atlantic Ocean). The first 10 kyr of these outputs are discarded for statistical analysis (described later in this study), as this initial part of the simulation is affected by the initial conditions (AMM10).

## 4. Results

Some results from the 1-Myr-long model solution are presented in this section. The spatiotemporal variability of atmospheric and oceanic variables, which arises in response to Milankovitch forcing, is described using principal component analysis (PCA; or empirical orthogonal function analysis). PCA decomposes the data into modes of variability that are standing oscillations. Hereafter, the $k$th component from a PCA performed on a variable $x$ is denoted as Ck($x$). The higher the component number $k$, the less the amount of total variance that component explains. If the standard deviation of $x$ is very large in a small region of the spatial domain (i.e., a few grid cells of the model), then C1($x$) simply replicates the large variability of this small region. This situation can be avoided by extracting the principal components from a correlation matrix, that is, by standardizing $x$ prior to PCA. Note, however, that the eigenvalues of the correlation matrix are not measures of the amount of variance explained by different principal components (Rencher 2002). Below, the variables are not standardized prior to PCA, unless stipulated otherwise.

### a. Surface air and ocean temperatures

In this section, the responses of annual and zonal means of surface air temperature ($T_a$), ocean mixed layer temperature ($T_m$, the mean temperature of the upper 70 m

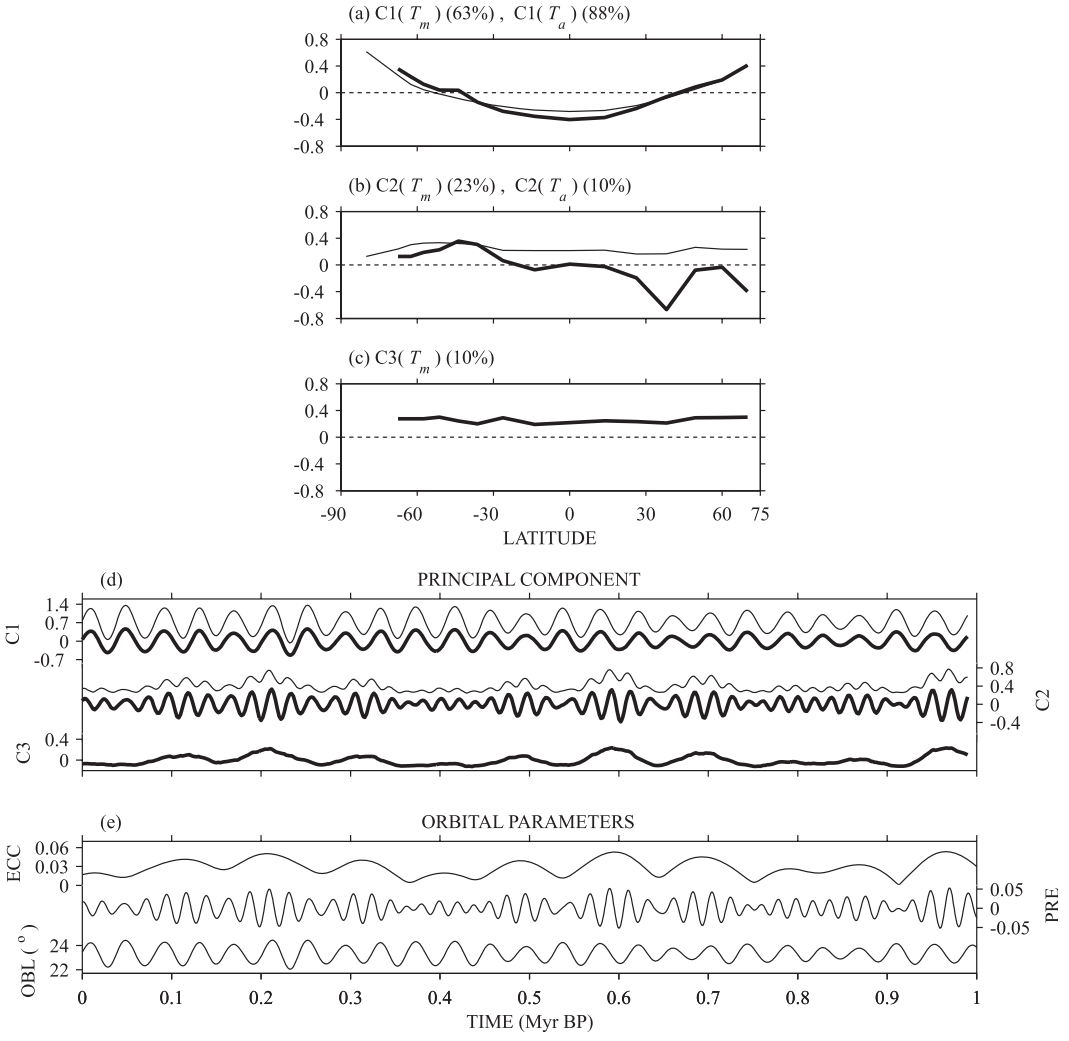


FIG. 2. Spatial patterns corresponding to the leading principal components (a) C1, (b) C2, and (c) C3 of annual-mean zonal-mean (over the global ocean) temperature of the ocean mixed layer ($T_m$, thick line) and annual-mean zonal-mean (over entire latitude circles) surface air temperature [$T_a$, thin line, C3($T_a$) not shown because it explains <2% of total variance]. (d) Corresponding time series where offsets of 0.7 and 0.4 have been added to C1($T_a$) and C2($T_a$), respectively, to better visualize the results. In (a)–(c), the fraction of total variance accounted for each component is shown in parentheses. (e) Time series of eccentricity (ECC), climatic precession parameter (PRE), and obliquity (OBL).

of the ocean), and ocean temperature ($T$) are described using PCA. Note that the model does not distinguish between sea surface temperature (SST) and $T_m$. Note also that $T_a$, $T_m$, and $T$ are zonally averaged over entire latitude circles, the global ocean, and different basins, respectively. Hence, $T_a$ and $T_m$ vary only with latitude, whereas $T$ is a function of latitude, depth, and ocean basin.

The atmospheric component C1($T_a$) (88% of total variance) is characterized by obliquity cycles that are in antiphase between low and high latitudes with a phase reversal near 40°S and 40°N (Figs. 2d and 2a). Mode C2($T_a$) (10%) is a combination of influences of eccentricity and precessional cycles, the eccentricity influence being dominant (Fig. 2d). The temperature changes associated with C2($T_a$) are in phase at all latitudes (Fig. 2b).

Overall, the ocean mixed layer component C1($T_m$) (63%) resembles the atmospheric component C1($T_a$) (Figs. 2a and 2d). Temperature changes associated with C2($T_m$) (23%) oscillate at precessional frequencies, with some modulation by eccentricity, and are in antiphase between hemispheres (Figs. 2d and 2b). Mode C3($T_m$) (10%) is characterized by eccentricity cycles that are in phase at all latitudes (Figs. 2d and 2c).

The oceanic component C1($T$) (72%) appears to be dominated by oscillations at precessional frequencies (Fig. 3d). The precessional influences in the deep Atlantic

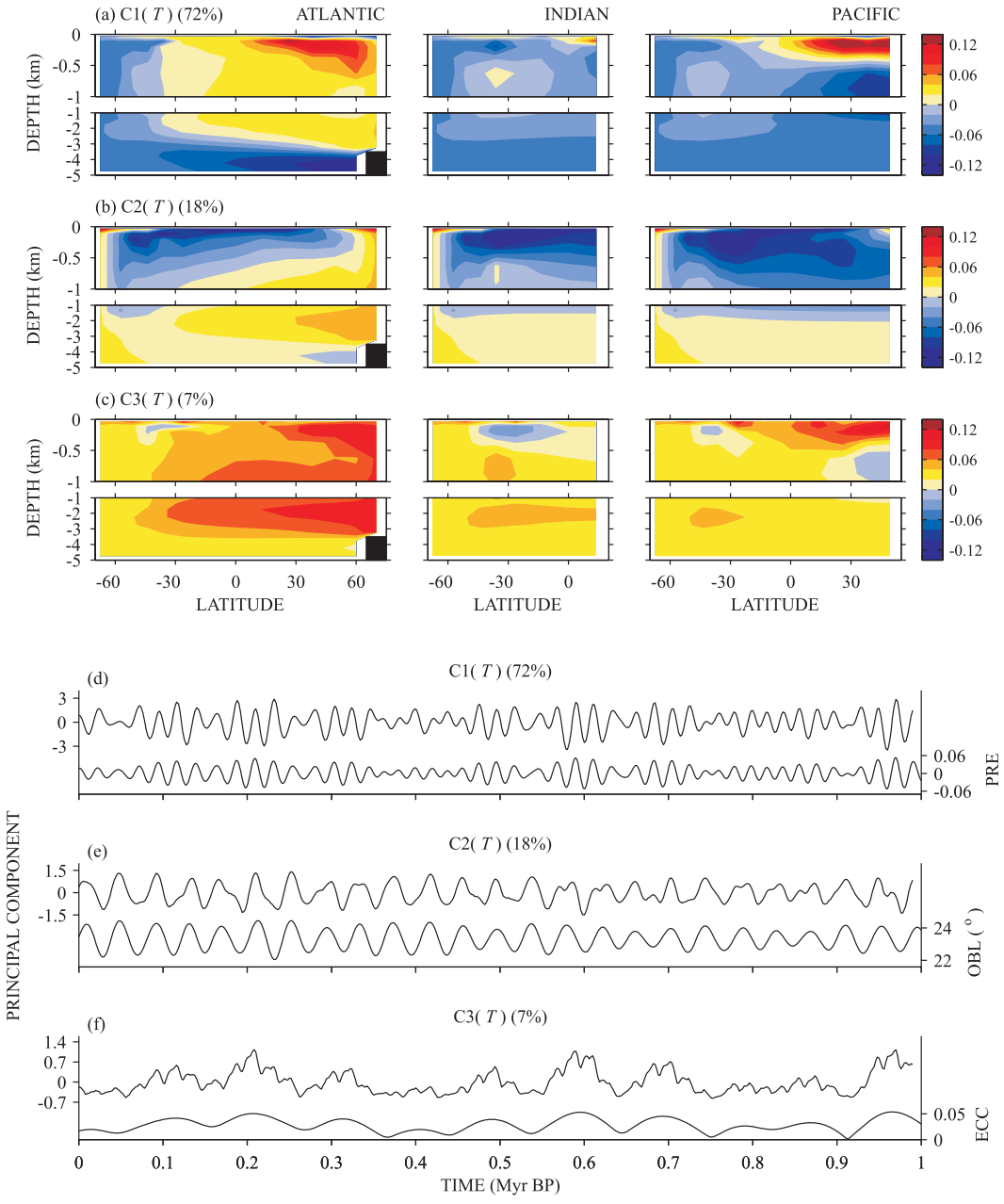


FIG. 3. (a)–(c) Spatial patterns and (d)–(f) time series corresponding to the leading principal components—(top to bottom) C1–C3—of annual- and zonal-mean ocean temperature in the (left to right) Atlantic, Indian, and Pacific Ocean basins. The fraction of total variance accounted for each component is shown in parentheses. The PRE, OBL, and ECC are also shown in (d),(e), and (f) with the vertical axis on the right.

Ocean (north of 30°S and above a depth of 3 km) and in the upper North Pacific Ocean (above a depth of 500 m) are in antiphase with those in the deep Indo-Pacific basin (below a depth of 1 km; Figs. 3a and 3d). The component C2($T$) (18%) is characterized by obliquity cycles that are in antiphase between low and high latitudes near the surface (Figs. 3e and 3b). These near-surface obliquity cycles of $T$ extend down to the seafloor at high latitudes (poleward of 60°S in the Southern Ocean and poleward of 60°N in the Atlantic Ocean) and to a depth of approximately 500–1000 m at lower latitudes (between 40°S and 40°N) (Fig. 3b). The mode C3($T$) (7%) consists of apparent eccentricity cycles that are in phase over most of the ocean (Figs. 3f and 3c).

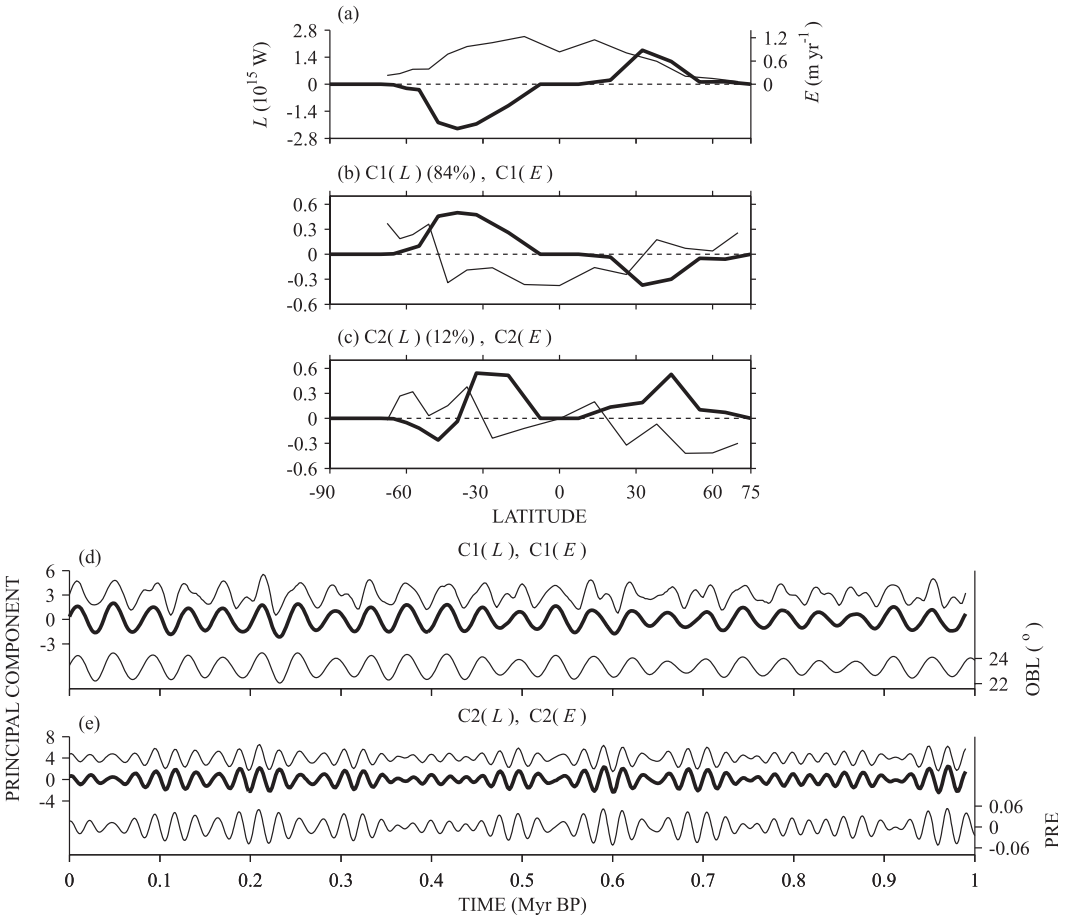


FIG. 4. (a) Latitudinal distributions of annual-mean zonal-mean (over entire latitude circles) evaporation ($E$, thin line) and meridional flux of latent heat in the atmosphere ($L$, thick line) averaged over the last 1 Myr. (b)–(c) Latitudinal distribution of the first and second principal components of $E$ (thin line) and $L$ (thick line). (d)–(e) Time series of the first two principal components of $E$ (thin line) and $L$ (thick line) normalized by their respective standard deviations. In (d)–(e), offsets of 3 and 4 have been added to C1($E$) and C2($E$), respectively, to better visualize the results. Positive and negative values of $L$ correspond to poleward latent heat transport in the Northern and Southern Hemispheres, respectively. Simulated changes in $L$ are less than $0.2 \times 10^{15}$ W. Hence, during the 1-Myr-long integration, the latitudinal distribution of $L$ remains very close to the time-averaged distribution shown in (a). In (b) and (c), the fraction of total variance accounted for C1($L$) and C2($L$) are given in parentheses. Such a fraction is not given for C1($E$) and C2($E$) because $E$ is standardized prior to PCA. In (d) and (e), OBL and PRE are also shown with the vertical axis on the right.

### *b. Hydrological cycle*

The spatiotemporal variability of annual and zonal means of meridional latent heat flux in the atmosphere ($L$) and of evaporation ($E$) is revealed below by PCA. We show results for $L$ and $E$ mainly because these two variables are invoked in the interpretation of deuterium excess records in terms of hydrological changes (see section 5b). Here values of annual- and zonal-mean $E$ are standardized prior to PCA.

The leading modes C1($L$) (84%) and C1($E$) are dominated by obliquity cycles (Fig. 4d). The largest changes in latent heat flux associated with C1($L$) occur at midlatitudes and are in antiphase between hemispheres (Fig. 4b). Because the poleward latent heat fluxes in the Southern and Northern Hemispheres have opposite signs, the antiphase relationship implies that the hydrological cycle is actually intensified or diminished in both hemispheres simultaneously. Component C1($E$) describes variations in evaporation that are in antiphase between low and high latitudes, with a phase reversal occurring near 40°S and 40°N (Fig. 4b).

The second modes C2($L$) (12%) and C2($E$) are dominated by precessional cycles (Fig. 4e). For C2($L$), the largest variability occurs between 20° and 32.5°S and at 43.8°N (Fig. 4c). Because the latent heat flux changes

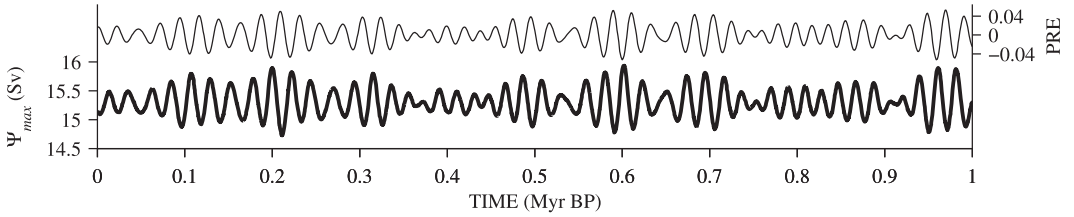


FIG. 5. Time series of the PRE (thin line) and maximum value of annual-mean meridional overturning in the North Atlantic Ocean below a depth of 500 m ($\Psi_{max}$, thick line).

associated with C2($L$) have the same sign in these two regions, the poleward flux of latent heat is intensified in one of these regions when it is diminished in the other (Fig. 4c). The evaporation changes described by C2($E$) tend to be in antiphase between hemispheres (Fig. 4c).

### c. *Fluxes of mass and heat in the ocean*

The changes in meridional mass and heat fluxes in the ocean as simulated in response to Milankovitch forcing are now considered.

In each ocean basin, the largest peak-to-peak variations of the maximum annual-mean streamfunction [$\Psi_{max}$, a measure of the strength of the meridional overturning circulation (MOC)] are about 1.5 Sv (1 Sv $\equiv 10^6$ m$^3$ s$^{-1}$). In particular, variations of $\Psi_{max}$ in the North Atlantic Ocean below a depth of 500 m are of the order of 1 Sv (Fig. 5). The time series of $\Psi_{max}$ nearly mirrors that of the climatic precession parameter (Fig. 5).

At every latitude, changes in vertically integrated oceanic meridional flux of heat (not shown) are typically less than 0.15 (0.25) $\times 10^{15}$ W in individual basins (in the global ocean). They mainly oscillate at precessional frequencies.

In summary, variations of meridional mass and heat fluxes in the ocean are not significant. Hence, in the time-dependent solution, the ocean circulation and its attendant meridional heat flux are always very close to those in the modern climate solution (see appendix).

## 5. Discussion

In this section, the main results obtained in this study are discussed from a mechanistic point of view. Emphasis is put on the simulated changes in (i) surface air and ocean temperatures, (ii) meridional flux of latent heat in the atmosphere, (iii) evaporation rate, and (iv) the MOC in the North Atlantic Ocean. Limitations and possible future extensions of this work are then discussed.

### a. *Temperature changes*

For the principal components, C1($T_a$), C1($T$), C2($T$), and C3($T$), the spatial patterns found in this work for the last 1 Myr are qualitatively similar to those found in a previous study for the 5–3 Myr BP time interval (AMM10; a version of our model with a fixed hydrological cycle was used in this earlier work). Furthermore, for each of these components, the time series shown in the present study and in AMM10 are similar in the frequency domain (the insolation changes for the last 1 Myr and for the 5–3 Myr BP time period are also similar in the frequency domain).

The similarity of our results with those of AMM10 implies that, on an annual- and zonal-mean basis, the responses of surface air temperature ($T_a$) and of ocean temperature ($T$) to Milankovitch forcing are not fundamentally modified by the inclusion of an active hydrological cycle. Thus, the interpretations of changes in $T_a$ and $T$ given by AMM10 also hold here.

The changes in $T_a$, $T_m$, and $T$ are interpreted as follows. Temperature variations near the obliquity frequency in our model are a response to annual-mean insolation. In particular, this forcing is the main control on annual- and zonal-mean $T_a$ and $T_m$. This is shown by the remarkable similarity between the spatiotemporal variability of C1($T_a$) and C1($T_m$) on the one hand (Figs. 2a and 2d) and that of annual-mean insolation on the other hand (changes in annual-mean insolation mostly oscillate at the obliquity frequency and are in antiphase between low and high latitudes with a phase reversal near 43°S and 43°N). At high latitudes, deep-water formation processes ''propagate'' variations of annual- and zonal-mean ocean mixed layer temperature near obliquity frequency to the deep ocean (i.e., below a depth of ca. 1000 m) (Fig. 3b). At low and midlatitudes, however, the vertical density stratification tends to inhibit such downward propagation (Fig. 3b).

Temperature changes at precessional frequencies are now discussed. Equatorward of polar circles (i.e., between 66°S and 66°N), precessionally driven changes in autumn–winter insolation (defined as in AMM10) generate precessional cycles of annual- and zonal-mean convective heat flux at the base of the ocean mixed layer (except near a polar circle, autumn–winter insolation changes are mostly driven by precession and are in

antiphase between hemispheres). Consequently, precessional cycles of annual- and zonal-mean temperature occur in subsurface ocean layers (i.e., in the 70–500-m-depth range; Fig. 3a) and, to a lesser degree, in the atmosphere–ocean-mixed-layer system (Fig. 2b). When these subsurface ocean temperature changes occur in regions of deep-water formation, for example, between 45° and 75°N in the Atlantic Ocean, precessional temperature cycles are introduced at depth (Fig. 3a).

Small-amplitude variations of annual- and zonal-mean air and ocean temperatures at eccentricity frequencies are in phase at most latitudes (Figs. 2b, 2c, and 3c). They are a response to small eccentricity-driven changes in annual-mean insolation, which are in phase at all latitudes.

As in AMM10, local air and ocean temperature changes in our land–ice-free model are always less than 2°C. These results are consistent with deep ocean temperature changes derived from paleoclimate records for the warm climate of the middle Pliocene (Dwyer et al. 1995; Cronin et al. 2005; see AMM10). On the other hand, as discussed in section 5d, the model underestimates air temperature changes inferred from ice-core data for the glacial–interglacial cycles of the late Pleistocene.

### b. Hydrological changes

Overall, the planetary-scale hydrological cycle mainly responds to obliquity, as shown by the leading principal components C1($L$) and C1($E$) (see section 4b). Note that C1($L$) captures a very large fraction (84%) of the total variance. According to Eq. (2), the magnitude of $L$ is approximately proportional to the square of the meridional gradient of air temperature. For this reason, an increase (decrease) in the magnitude of $L$ in C1($L$) corresponds to an enhancement (diminishing) of the low-to-high-latitude contrast of air temperature in C1($T_a$) due to low (high) obliquity. The response of evaporation to obliquity described by C1($E$) is similar to that of air and ocean mixed layer temperatures. Hence, evaporation changes are interpreted exactly the same way as these temperature variations (see section 5a).

Interestingly, the strong response of the hydrological cycle to obliquity found in our simplified model is consistent with an interpretation by Vimeux et al. (1999, 2001a) of the dominant obliquity cycles observed in deuterium excess records from polar ice (see Fig. 1). According to these authors, in both hemispheres, an increased equator-to-pole difference in annual-mean insolation during low obliquity would increase (decrease) the SST and the evaporation rate at low (high) latitudes (Fig. 6, upper panel). Thus, the poleward transport of moisture in the atmosphere ($L$) would intensify (Fig. 6, upper panel). Consequently, the deuterium excess of polar precipitation would increase as the relative contribution

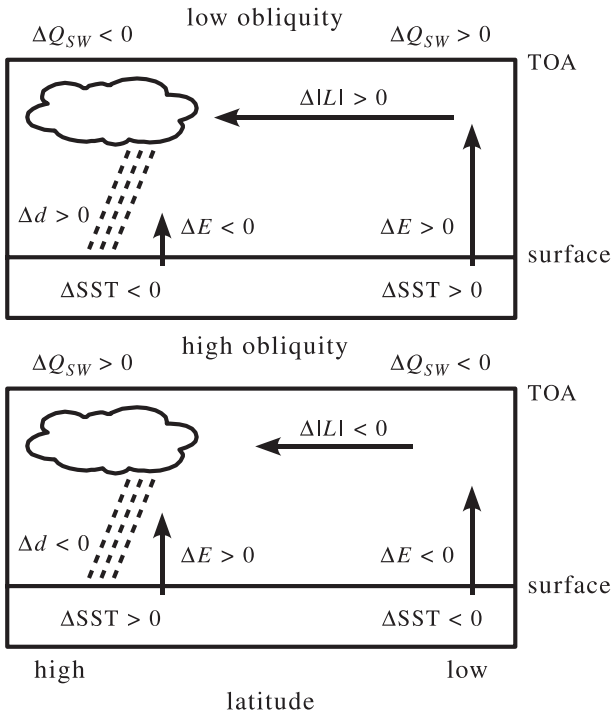


FIG. 6. Schematic rendering of the atmosphere–surface-ocean system depicting the hydrological changes invoked by Vimeux et al. (1999, 2001a) to interpret obliquity cycles observed in deuterium excess records from polar ice cores. Obliquity variations produce changes in annual-mean insolation ($\Delta Q_{SW}$), sea surface temperature ($\Delta SST$), evaporation rate ($\Delta E$), magnitude of poleward latent heat flux ($\Delta|L|$), and deuterium excess of polar precipitation ($\Delta d$). This corresponds to a situation in which (top) low [(bottom) high] obliquity increases (decreases) the low-to-high-latitude contrast in annual-mean insolation at the ''top of the atmosphere'' (TOA).

of low latitudes to polar precipitation is enhanced compared to that of high latitudes (Fig. 6, upper panel). Opposite changes would occur in the case of high obliquity (Fig. 6, lower panel). These responses of SST, evaporation rate, and $L$ to obliquity changes are found in our leading principal components C1($T_m$), C1($E$), and C1($L$) and time series of model variables (Fig. 7), which provides support to the interpretation of Vimeux et al. (1999, 2001a). Note, however, that an explicit simulation of deuterium excess would be necessary to test more rigorously this interpretation.

A role of obliquity in long-term hydrological changes as observed in our time-dependent solution was also found in two previous snapshot simulations performed with atmosphere–ocean general circulation models (AOGCMs). First, Khodri et al. (2001) forced an AOGCM with insolation values at 115 kyr BP (last glacial inception) when obliquity was lower than its modern value (i.e., the equator-to-pole contrast of annual-mean insolation was large compared to today). In this simulation, the

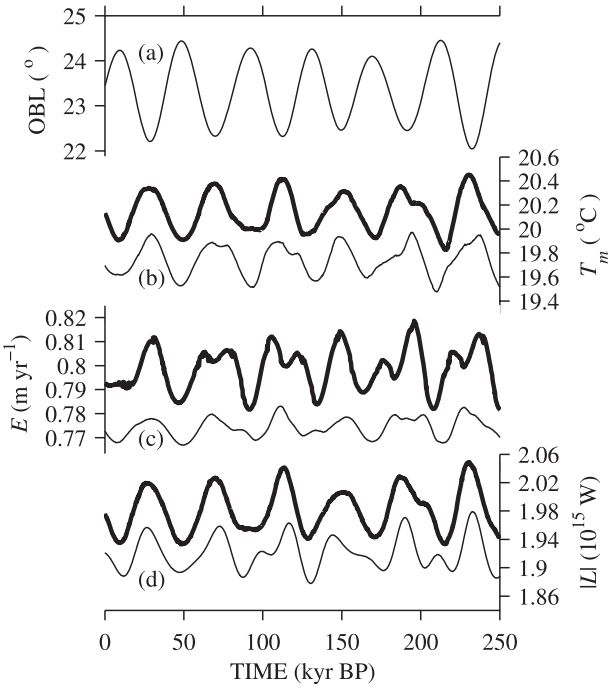


FIG. 7. Time series (for the last 250 kyr of the run) of (a) obliquity and low-to-high-latitude difference in annual-mean–zonal-mean (b) temperature of the ocean mixed layer (zonal mean over the global ocean) and (c) evaporation (zonal mean over entire latitude circles); and (d) magnitude of annual-mean poleward latent heat flux in the atmosphere at midlatitudes. In (b) and (c), the thick (thin) line corresponds to differences between values at 26.25° and 62.5°S (26.25° and 60°N). In (d), the thick (thin) line shows changes at 47.5°S (43.8°N). To better visualize the results, the Northern Hemisphere values [the thin lines in (b)–(d)] have been increased by 5.6°C, 0.115 m yr$^{-1}$, and $0.75 \times 10^{15}$ W in (b), (c), and (d), respectively.

annual-mean poleward transport of latent heat in the atmosphere at northern mid- and high latitudes is enhanced compared to modern conditions. However, in the numerical experiment of Khodri et al. (2001) and ours, changes in annual- and zonal-mean atmospheric meridional transport of latent heat are less than $0.2 \times 10^{15}$ W. Second, Vimeux et al. (2001b) analyzed two simulations (present day and 6 kyr BP, when obliquity was larger than today) performed with an AOGCM (Braconnot et al. 1997, 2000). They found that, in the Southern Hemisphere, low-to-high-latitude contrasts of annual- and zonal-mean evaporation and SST at 6 kyr BP are smaller than at present. As in Vimeux et al. (2001b), our simulated variations of annual- and zonal-mean evaporation are less than 0.1 m yr$^{-1}$. In the model used by Braconnot et al. (1997, 2000) and our model, the variations of zonal averages of evaporation and SST across different ocean basins (not shown) are similar to those of zonal averages across the global ocean. This zonal uniformity may exist because of the lack of longitudinal resolution in the atmospheric component of our model. However, it is not necessarily expected in a three-dimensional model such as used by Braconnot et al. (1997, 2000).

Hydrological changes at precessional frequencies also occur in our numerical experiment [e.g., see the principal components C2($L$) and C2($E$) described in section 4b]. These changes are apparently related to the responses of surface air and sea surface temperatures to precessional forcing (section 4a). However, these changes driven by precession do not warrant further discussion, as they do not dominate the variability of hydrological variables.

In summary, the hydrological cycle in our simulation is mostly controlled by obliquity-driven changes in the meridional gradient of annual-mean insolation. This result is consistent with long-term variability of deuterium excess records from polar ice cores and with numerical experiments with AOGCMs.

### c. *Changes in the Atlantic MOC*

As discussed previously (sections 5a and 5b), the meridional gradient of SST and meridional moisture flux in the atmosphere mainly respond to obliquity. Hence, one may expect to find that the North Atlantic MOC is also controlled by obliquity. However, the North Atlantic circulation mainly responds to precession (see Fig. 5). This counterintuitive response is explained as follows. When the climatic precession parameter is low, the autumn–winter insolation is decreased in the Northern Hemisphere. Consequently, in the North Atlantic Ocean and south of the polar circle, the temperature also decreases in the 70–500-m-depth range (section 5a). These subsurface temperature changes, in turn, enhance the low-to-high-latitude contrast of subsurface ocean temperature in the North Atlantic Ocean (Fig. 3a). These changes are accompanied by changes in the subsurface meridional gradient of density, so the MOC in the North Atlantic Ocean is strengthened when the climatic precession parameter is low (Fig. 5). Changes with opposite sign occur when the climatic precession parameter is high.

The response of Atlantic MOC to precession as described above was also found by Crucifix and Loutre (2002), who forced a zonally averaged climate model with insolation changes between 126 and 115 kyr BP (i.e., the last interglacial). In agreement with our results, these authors found that the Atlantic MOC is more sensitive to precession than to obliquity. Note that several components of the climate system that are not represented in our model (e.g., atmospheric circulation, sea ice, and continental vegetation) are included in the model of Crucifix and Loutre (2002). Although the Atlantic MOC responds to precession in our model, it is important to remark that simulated changes in Atlantic

MOC (and in the meridional heat flux in the Atlantic Ocean) are small (section 4c). A weak response of the MOC to Milankovitch forcing was also found in a previous version of our model with a fixed hydrological cycle (AMM10).

Small changes of the MOC in the Atlantic Ocean have also been found in earlier numerical studies concerning the response of a warm climate (i.e., with negligible ice volume on land) to Milankovitch forcing. Brickman et al. (1999) performed a 3.2-Myr-long simulation with a zonally averaged ocean–atmosphere model and found that changes in the maximum meridional overturning in the North Atlantic Ocean are smaller than 1 Sv. A fixed hydrological cycle was used in this previous study. In the much shorter 11-kyr-long simulation of Crucifix and Loutre (2002), changes in the export of deep water of North Atlantic origin to the Southern Ocean are less than 2 Sv. In the model study of Khodri et al. (2001), differences in the Atlantic meridional overturning streamfunction between 115 kyr BP and modern conditions are smaller than 3 Sv below a depth of 500 m.

To sum up, whereas we find that the Atlantic MOC responds to precession, our study and previous numerical experiments on warm climate suggest that the MOC responds weakly to Milankovitch forcing.

### *d. Limitations and perspectives*

The results of the present study should be interpreted in the context of an idealized model in which several processes are deliberately omitted. Hence, although some qualitative comparisons between model output and paleoclimate data appear legitimate (e.g., deuterium excess data from ice cores; section 5b), our model is not expected to explain such data in detail. Indeed, the model does not reproduce several features observed in the temperature records from Antarctic ice cores (Petit et al. 1999; Jouzel et al. 2007). For instance, the large-amplitude 100-kyr cycles found in these records are not present in our temperature responses to insolation changes. Our simulated temperature changes in the atmosphere are less than 2°C and, therefore, are much smaller than the glacial–interglacial changes in air temperature derived from ice cores. Most likely, these differences between model results and ice-core data exist because our model lacks a land–ice component and associated climate processes (e.g., the land–ice albedo feedback and the effect of the ice sheet elevation on surface air temperature). The differences could also be related to the absence of other climatic processes in the model such as changing winds, terrestrial vegetation–albedo feedback, and varying concentrations of greenhouse gases in the atmosphere.

It is also important to note that our model only simulates changes at the planetary scale. Thus, for instance, we do not consider the possibility of a strong response of regional ocean dynamics to Milankovitch forcing that can lead to important climate changes at specific locations. Such a significant climatic response at regional scales was found by Khodri et al. (2001) in an AOGCM.

Nevertheless, results from our idealized experiments may provide a useful framework for future and more complete simulations of the time-dependent climatic response to Milankovitch forcing. A continuation of this work would consist of assessing the sensitivity of model results to changes in parameterization; for instance, it would be useful to consider different representations of atmospheric heat transport and ocean mixing. Another possible extension of this work would be to include other components of the climate system (e.g., land ice sheets, sea ice, changing winds, and the carbon cycle) in the model. This extended model could then be used to perform more credible simulations of the climatic response to Milankovitch forcing over the last 1 Myr.

## 6. Conclusions

The zonally averaged ocean–atmosphere model developed in AMM10 is extended to include an active hydrological cycle. The extended model is integrated under the influence of Milankovitch forcing for the last 1 Myr. Our main conclusions are the following:

(i) The inclusion of an active hydrological cycle in the model does not significantly modify the responses of surface air and ocean temperatures to insolation changes found in a previous numerical experiment with a fixed hydrological cycle (AMM10).

(ii) The annual- and zonal-mean state of the planetary-scale hydrological cycle mainly responds to obliquity. When the equator-to-pole contrast of annual-mean insolation is enhanced (diminished), owing to low (high) obliquity, the poleward transport of moisture in the atmosphere is intensified (weakened). These results are consistent with dominant obliquity cycles observed in deuterium excess records from polar ice cores, which are believed to reflect changes in the large-scale hydrological cycle (Vimeux et al. 1999, 2001a).

(iii) In contrast to the hydrological response, the North Atlantic MOC mainly responds to precessionally driven variations of ocean temperature. However, the MOC exhibits small changes in every basin.

(iv) On an annual- and zonal-mean basis, the atmosphere–ocean response to Milankovitch forcing found in our time-dependent solution of a simplified model is generally consistent with that obtained from snapshot simulations performed with three-dimensional models.

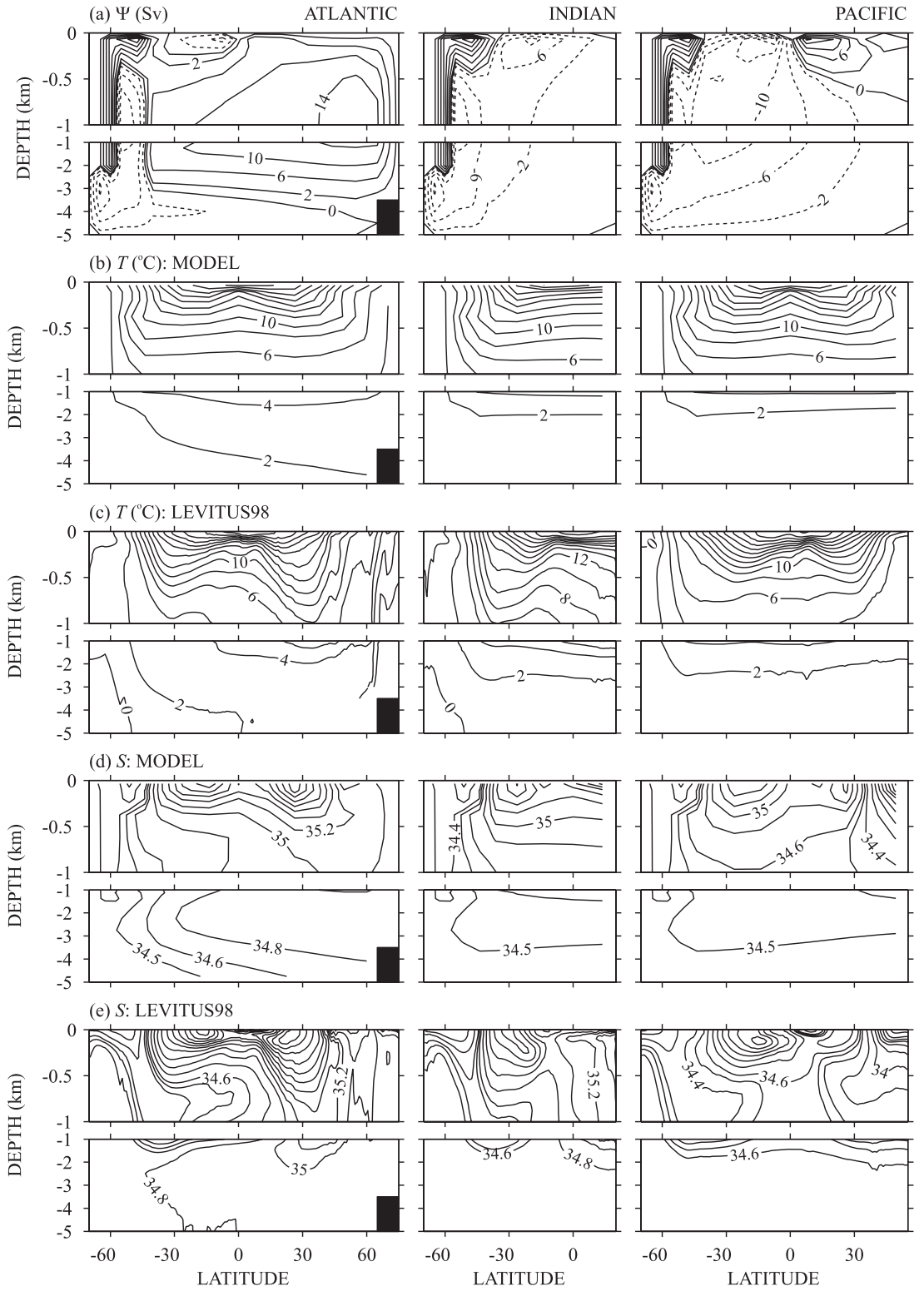


FIG. A1. Latitude–depth distributions of zonal and annual means of (a) streamfunction (Ψ), (b) model temperature, (c) Levitus98 temperature, (d) model salinity, and (e) Levitus98 salinity in the (left to right) Atlantic, Indian, and Pacific Ocean basins. In (a), (b), and (d), model variables averaged over the last 100 yr of a modern climate solution are shown (see appendix). In (c) and (e), annual climatological means are shown (National Oceanographic Data Center 1998). In (a), clockwise (counterclockwise) circulation is depicted by solid (dashed) contours. For Ψ, the contour interval is 2 Sv for values between −2 and 2 Sv, and 4 Sv otherwise. The contour interval for temperature (salinity) is 2°C (0.2 PSU). In (d),(e), the contour of 34.5 PSU is also shown.

We stress that our idealized experiment is not meant to be an accurate simulation of the response of climate to insolation changes. Instead, it is intended to shed light on some fundamental aspects of this climatic response. Our results should thus be viewed as a step toward understanding the role of different climatic elements (e.g., the planetary hydrological cycle) in the time-dependent response of the earth system to Milankovitch forcing.

*Acknowledgments.* We are grateful to V. Masson-Delmotte for useful discussions and to three anonymous reviewers for their constructive comments that greatly improved the manuscript. National Oceanographic Data Center 1998 data and NCEP Reanalysis data were provided by the NOAA/OAR/ESRL PSD, Boulder, Colorado, from their Web site (available online at http://www.cdc.noaa.gov/). A. A. thanks the Global Environmental and Climate Change Centre of McGill University for a Network Grant that made possible an enriching two-week stay at WHOI during June 2007. O. M. acknowledges support from the U.S. National Science Foundation. Support from a Canadian NSERC Discovery Grant awarded to L.A.M. is gratefully acknowledged. This paper is dedicated to the memory of Daniel Wright, whose contribution to the development of zonally averaged models in physical oceanography benefited us all.

## APPENDIX

### Model Solution for Modern Climate

This solution is produced using the spinup procedure of AMM10 with minor modifications. The two stages of this model spinup are briefly described here, with emphasis on the changes introduced in this study.

During the first stage (5-kyr-long spinup of ocean model with restoring boundary conditions), the restoring temperature ($T^*$) and salinity ($S^*$) values are modified to decrease model–observation differences in the distributions of temperature and salinity. Unlike in AMM10, the modifications to $T^*$ and $S^*$ are as follows: (i) $S^*$ is increased by 0.3 between 55° and 75°N in the Atlantic Ocean and between 70° and 55°S in the Southern Ocean, and (ii) $T^*$ is increased by 3°C between 32.5° and 55°N in the Pacific Ocean. These salinity anomalies superimposed on the high-latitude $S^*$ are similar to those used in other ocean models (e.g., Stocker et al. 1992a; Schmittner and Stocker 2001). As in Stocker et al. (1992b), we increase $T^*$ in the North Pacific Ocean to avoid the occurrence of deep-water formation in this basin after the ocean model is coupled to the atmospheric component. Note, however, that our imposed North Pacific $T^*$ anomaly is much larger than that of Stocker et al. (1992b) (0.2°C). This can be attributed to differences between the model of Stocker et al. (1992b) and ours (e.g., differences in the values of mixing coefficients for temperature and salinity and differences in model geometry).

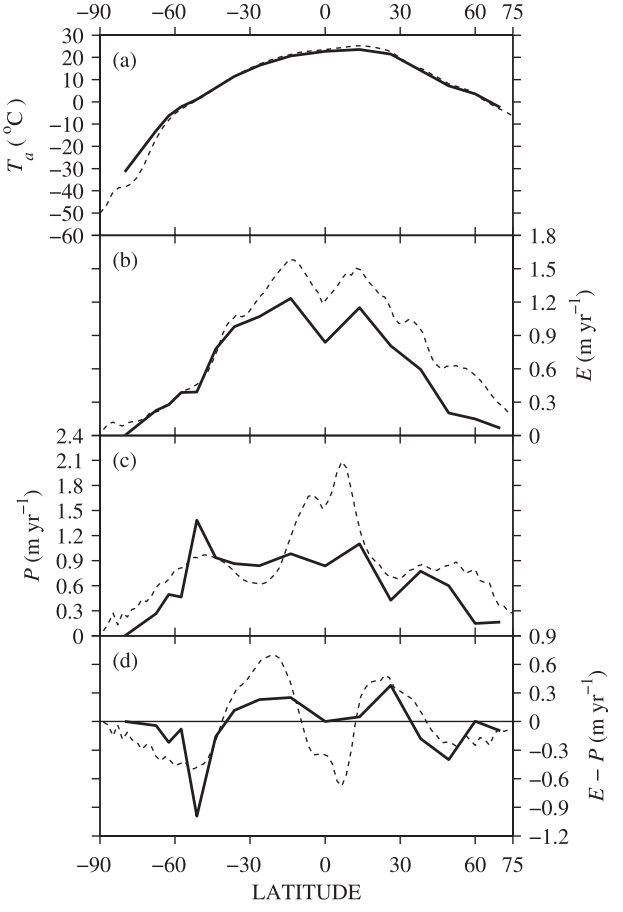


FIG. A2. Latitudinal distributions of annual and zonal means of (a) surface air temperature, (b) evaporation, (c) precipitation, and (d) evaporation minus precipitation. In (a)–(d), variables are zonally averaged over entire latitude circles. The solid lines show model values averaged over the last 100 yr of a modern climate solution (see appendix). The dashed lines show reanalysis estimates (Kalnay et al. 1996).

In the second stage (7-kyr-long coupled run), the atmospheric energy balance model and the active hydrological cycle model are coupled to the ocean model. Various model outputs averaged over the last 100 yr of this stage are described here.

The latitude–depth distributions of annual-mean streamfunction for the different ocean basins are shown in Fig. A1a. The Atlantic circulation is consistent in magnitude and spatial structure with that obtained from other models, including three-dimensional ocean models (Doney et al. 2004). The maximum annual-mean meridional overturning in the North Atlantic below a depth of 500 m is about 15.2 Sv, which is consistent with the volume

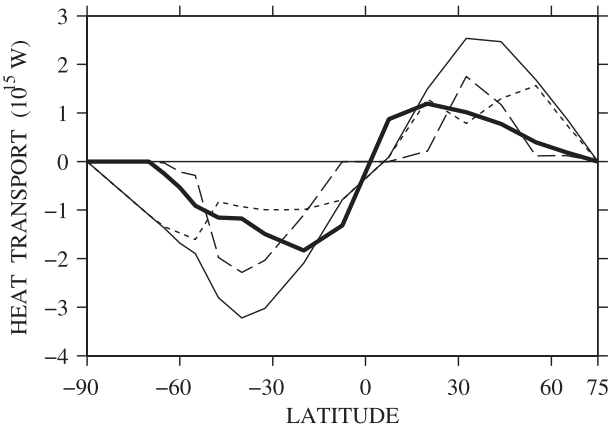


FIG. A3. Latitudinal distributions of annual means of atmospheric meridional transport of sensible heat and potential energy (short dashed line), atmospheric meridional transport of latent heat (long dashed line), total meridional heat transport in the atmosphere (thin solid line), and total meridional heat transport in the global ocean (thick solid line). These annual means are averaged over the last 100 yr of a modern climate solution (see appendix). Positive (negative) values correspond to poleward transport in the Northern (Southern) Hemisphere.

transport of 17 Sv estimated from hydrographic sections near 25°N in this basin (Roemmich and Wunsch 1985).

The root-mean-square differences between climatological (National Oceanographic Data Center 1998) and model annual means of global ocean temperature and salinity are about 1.01°C and 0.20, respectively. These values are similar to those reported in AMM10 and are also within the range of values for several ocean circulation models (Doney et al. 2004). Overall, the model can reproduce major features of the climatological distributions of temperature and salinity in each basin (Figs. A1b–e).

Likewise, outputs from the atmospheric component of our model compare favorably with the reanalysis estimates from the National Centers of Environmental Prediction (NCEP; Kalnay et al. 1996) pertaining to modern climate (Fig. A2). The latitudinal distributions of annual- and zonal-mean surface air temperature and evaporation rate are in good agreement with climatology (Figs. A2a and A2b); although the model underestimates evaporation rates north of 30°S. The agreement between the simulated and NCEP values of precipitation is also reasonable outside of the tropics, where the model reproduces the precipitation maxima at midlatitudes (Fig. A2c). However, the model does not simulate the large precipitation maximum observed near the equator in the NCEP reanalysis (Fig. A2c). This is mainly because our model does not contain a representation of the moisture convergence near the equator that is due to the atmospheric circulation patterns (e.g., Hadley cell circulation). For the same reason, the negative values of evaporation minus precipitation in the tropics are not reproduced by the model (Fig. A2d). Elsewhere, the difference between evaporation and precipitation simulated by the model has realistic sign and magnitude (Fig. A2d).

Finally, our model simulates total meridional heat transports in the atmosphere (Fig. A3, thin solid line) and in the global ocean (Fig. A3, thick solid line), which are in reasonable agreement with those estimated by Wunsch (2005). Similarly, the simulated atmospheric meridional transports of sensible heat and potential energy (Fig. A3, short dashed line) and of latent heat (Fig. A3, long dashed line) are comparable with the observational estimates of Schmittner et al. (2000) at every latitude, except in the tropics where the model does not replicate the observed moisture convergence near the equator.

## REFERENCES

Antico, A., O. Marchal, and L. A. Mysak, 2010: Time-dependent response of a zonally averaged ocean–atmosphere–sea ice model to Milankovitch forcing. *Climate Dyn.,* **34,** 763–779.

Berger, A. L., 1978: Long-term variations of daily insolation and quaternary climate changes. *J. Atmos. Sci.,* **35,** 2362–2367.

——, and M. F. Loutre, 1991: Insolation values for the climate of the last 10 million years. *Quat. Sci. Rev.,* **10,** 297–317.

Bjornsson, H., L. A. Mysak, and G. Schmidt, 1997: Mixed boundary conditions versus coupling with an energy–moisture balance model for a zonally averaged climate model. *J. Climate,* **10,** 2412–2430.

Braconnot, P., O. Marti, and S. Joussaume, 1997: Adjustments and feedbacks in a global coupled ocean–atmosphere model. *Climate Dyn.,* **13,** 507–519.

——, ——, and ——, 2000: Ocean feedback in response to 6 kyr BP insolation. *J. Climate,* **13,** 1537–1553.

Brickman, D., W. Hyde, and D. G. Wright, 1999: Filtering of Milankovitch cycles by the thermohaline circulation. *J. Climate,* **12,** 1644–1658.

Cronin, T. M., H. J. Dowsett, G. S. Dwyer, P. A. Baker, and M. A. Chandler, 2005: Mid-Pliocene deep-sea bottom-water temperatures based on ostracode Mg/Ca ratios. *Mar. Micropaleontol.,* **54,** 249–261.

Crucifix, M., and M. F. Loutre, 2002: Transient simulations over the last interglacial period (126–115 kyr BP): Feedback and forcing analysis. *Climate Dyn.,* **19,** 417–433.

——, ——, and A. Berger, 2006: The climate response to the astronomical forcing. *Space Sci. Rev.,* **125,** 213–226.

Doney, S. C., and Coauthors, 2004: Evaluating global ocean carbon models: The importance of realistic physics. *Global Biogeochem. Cycles,* **18,** GB3017, doi:10.1029/2003GB002150.

Dwyer, G. S., T. M. Cronin, P. A. Baker, M. E. Raymo, J. S. Buzas, and T. Corrège, 1995: North Atlantic deepwater temperature change during late Pliocene and late Quaternary climatic cycles. *Science,* **270,** 1347–1351.

Jouzel, J., and Coauthors, 2007: Orbital and millennial Antarctic climate variability over the past 800 000 years. *Science,* **317,** 793–796.

Kalnay, E., and Coauthors, 1996: The NCEP/NCAR 40-Year Reanalysis Project. *Bull. Amer. Meteor. Soc.,* **77,** 437–471.

Khodri, M., Y. Leclainche, G. Ramstein, P. Braconnot, O. Marti, and E. Cortijo, 2001: Simulating the amplification of orbital forcing by ocean feedbacks in the last glaciation. *Nature,* **410,** 570–574.

Lisiecki, L. E., and M. E. Raymo, 2005: A Pliocene–Pleistocene stack of 57 globally distributed benthic $\delta^{18}O$ records. *Paleoceanography,* **20,** PA1003, doi:10.1029/2004PA001071.

——, and ——, 2007: Plio–Pleistocene climate evolution: Trends and transitions in glacial cycle dynamics. *Quat. Sci. Rev.,* **26,** 56–59.

Loutre, M. F., D. Paillard, F. Vimeux, and E. Cortijo, 2004: Does mean annual insolation have the potential to change the climate? *Earth Planet. Sci. Lett.,* **221,** 1–14.

Masson-Delmotte, V., and Coauthors, 2005: GRIP deuterium excess reveals rapid and orbital-scale changes in Greenland moisture origin. *Science,* **309,** 118–121.

National Oceanographic Data Center, cited 1998: NODC (Levitus) World Ocean Atlas 1998. [Available online at http://www.esrl.noaa.gov/psd/data/gridded/data.nodc.woa98.html.]

Paillard, D., 2001: Glacial cycles: Toward a new paradigm. *Rev. Geophys.,* **39,** 325–346.

Park, J., and R. J. Oglesby, 1990: A comparison of precession and obliquity effects in a Cretaceous paleoclimate simulation. *Geophys. Res. Lett.,* **17,** 1929–1932.

Petit, J. R., and Coauthors, 1999: Climate and atmospheric history of the past 420 000 years from the Vostok ice core, Antarctica. *Nature,* **399,** 429–436.

Rencher, A. C., 2002: Principal component analysis. *Methods of Multivariate Analysis,* John Wiley & Sons, 380–407.

Rind, D., 1998: Latitudinal temperature gradients and climate change. *J. Geophys. Res.,* **103,** 5943–5971.

Roemmich, D., and C. Wunsch, 1985: Two transatlantic sections: Meridional circulation and heat flux in the subtropical North Atlantic Ocean. *Deep-Sea Res.,* **32,** 619–664.

Schmittner, A., and T. F. Stocker, 1999: The stability of the thermohaline circulation in global warming experiments. *J. Climate,* **12,** 1117–1133.

——, and ——, 2001: A seasonally forced ocean–atmosphere model for paleoclimate studies. *J. Climate,* **14,** 1055–1068.

——, C. Appenzeller, and T. F. Stocker, 2000: Validation of parameterizations for the meridional energy and moisture transport used in simple climate models. *Climate Dyn.,* **16,** 63–77.

Short, D. A., J. G. Mengel, T. J. Crowley, W. T. Hyde, and G. R. North, 1991: Filtering of Milankovitch cycles by Earth's geography. *Quat. Res.,* **35,** 157–173.

Stocker, T. F., D. G. Wright, and W. S. Broecker, 1992a: The influence of high latitude forcing on the global thermohaline circulation. *Paleoceanography,* **7,** 529–541.

——, ——, and L. A. Mysak, 1992b: A zonally averaged, coupled ocean–atmosphere model for paleoclimate studies. *J. Climate,* **5,** 773–797.

Stone, P. H., and D. A. Miller, 1980: Empirical relations between seasonal changes in meridional temperature gradients and meridional fluxes of heat. *J. Atmos. Sci.,* **37,** 1708–1721.

Tiedemann, R., M. Sarnthein, and N. J. Shackleton, 1994: Astronomic timescale for the Pliocene Atlantic $\delta^{18}O$ and dust flux records of Ocean Drilling Program site 659. *Paleoceanography,* **9,** 619–638.

Valdes, P. J., and R. W. Glover, 1999: Modelling the climate response to orbital forcing. *Philos. Trans. Roy. Soc. London,* **A357,** 1873–1890.

——, B. W. Sellwood, and G. D. Price, 1995: Modelling Late Jurassic Milankovitch climate variations. *Geol. Soc. London, Spec. Publ.,* **85,** 115–132.

Vimeux, F., V. Masson, J. Jouzel, M. Stievenard, and J. R. Petit, 1999: Glacial–interglacial changes in ocean surface conditions in the Southern Hemisphere. *Nature,* **398,** 410–413.

——, ——, G. Delaygue, J. Jouzel, J. R. Petit, and M. Stievenard, 2001a: A 420 000 year deuterium excess record from East Antarctica: Information on past changes in the origin of precipitation at Vostok. *J. Geophys. Res.,* **106,** 31 863–31 873.

——, ——, J. Jouzel, J. R. Petit, E. J. Steig, M. Stievenard, R. Vaikmae, and J. W. C. White, 2001b: Holocene hydrological cycle changes in the Southern Hemisphere documented in east Antarctic deuterium excess records. *Climate Dyn.,* **17,** 503–513.

Wright, D. G., and T. F. Stocker, 1992: Sensitivities of a zonally averaged global ocean circulation model. *J. Geophys. Res.,* **97,** 12 707–12 730.

Wunsch, C., 2005: The total meridional and heat flux and its oceanic and atmospheric partition. *J. Climate,* **18,** 4374–4380.

Young, M. A., and R. S. Bradley, 1984: Insolation gradients and the paleoclimatic record. *Milankovitch and Climate, Part 2,* A. Berger et al., Eds., D. Reidel, 707–713.